

# Real-time four-dimensional optical-resolution photoacoustic microscopy with Au nanoparticle-assisted subdiffraction-limit resolution

Bin Rao,<sup>1</sup> Konstantin Maslov,<sup>1</sup> Amos Danielli,<sup>1</sup> Ruimin Chen,<sup>2</sup> K. Kirk Shung,<sup>2</sup> Qifa Zhou,<sup>2</sup> and Lihong V. Wang<sup>1,\*</sup>

<sup>1</sup>Department of Biomedical Engineering, Optical Imaging Lab, Washington University in St. Louis, Campus Box 1097, One Brookings Drive, St. Louis, Missouri 63130-4899, USA

<sup>2</sup>Department of Biomedical Engineering, University of Southern California, Los Angeles, California 90089, USA

\*Corresponding author: lhwang@biomed.wustl.edu

Received January 19, 2011; revised February 23, 2011; accepted February 25, 2011; posted March 3, 2011 (Doc. ID 140483); published March 23, 2011

Photoacoustic microscopy (PAM) offers label-free, optical absorption contrast. A high-speed, high-resolution PAM system in an inverted microscope configuration with a laser pulse repetition rate of 100,000 Hz and a stationary ultrasonic transducer was built. Four-dimensional *in vivo* imaging of microcirculation in mouse skin was achieved at 18 three-dimensional volumes per second with repeated two-dimensional (2D) raster scans of 100 by 50 points. The corresponding 2D B-scan (50 A-lines) frame rate was 1800 Hz, and the one-dimensional A-scan rate was 90,000 Hz. The lateral resolution is  $0.23 \pm 0.03 \mu\text{m}$  for Au nanowire imaging, which is 2.0 times below the diffraction limit. © 2011 Optical Society of America

OCIS codes: 170.3880, 170.5120, 180.5810, 110.5120, 110.0180.

Modern optical microscopes are indispensable tools for life scientists to visualize the morphological details of cellular and subcellular anatomy, comprehend fundamental biological processes, and solve biological problems. Optical-resolution photoacoustic microscopy (OR-PAM), a major method of photoacoustic tomography (PAT) [1,2], has been recognized as a novel, optical microscopic method with excellent, label-free optical absorption contrast and high lateral resolution [3–7]. The absorption contrast enables imaging of nonfluorescent molecules.

In OR-PAM, transient acoustic waves are generated by laser-induced thermal expansion when nanosecond laser pulse energy is deposited into a focal volume of biological tissue [3]. Hemoglobin in blood, as well as melanin in skin, hair, iris, retina tissues, etc., produces excellent endogenous contrast [8–10]. Functional PAT based on either the quantitative oxygen-saturation measurement of hemoglobin or the flow speed measurement of red blood cells (RBCs) further extends the contrast mechanisms for *in vivo* biomedical imaging [11,12]. The conjugation of weakly fluorescent, low-scattering, low-absorbing, endogenous targets in nonpigmented cells with exogenous contrast agents, such as gold nanoparticles, promises *in vivo* detection of circulating cancer cells [13]. A recently reported submicrometer-resolution OR-PAM system expanded the scope to cellular and subcellular organelles [7]. In this Letter, we demonstrate a high-resolution OR-PAM system with almost 2 orders of magnitude of imaging speed improvement over our previously reported submicrometer OR-PAM system [7] and less than 3 dB PA signal loss within its entire imaging field of view (FOV).

The schematic of our imaging system is shown in Fig. 1. For cellular imaging applications, the small imaging FOV and the access to both sides of tissue samples favor this system design with two-dimensional (2D) optical scan and a single, stationary ultrasonic transducer. A pulsed

laser (532 nm wavelength  $\lambda$ , 2 ns pulse duration, and 100 kHz pulse repetition rate) was used as the light source. It was generated from a second harmonic crystal (KTP) by a diode-pumped, actively E-O Q-switched Nd:YVO<sub>4</sub> laser operating at the 1064 nm wavelength. A 2D Galvo system scanned the collimated laser beam pivotally through the pupil of the optical objective (Olympus LCPlanFI, 0.6 NA, infinity corrected). Two achromatic lenses (75 mm focal length) formed a standard 4-f system that imaged the scanning Galvo mirrors to the pupil location of the objective. The system was designed in an inverted microscope configuration with the sample illuminated by the laser beam from the bottom. The excited PA signal was detected by a stationary ultrasonic transducer through water coupling.

Two types of stationary, ultrasonic transducers were custom built according to the trade-off between imaging FOV and detection sensitivity. The nonfocused transducer (lead magnesium niobate–lead titanate single crystal) had an effective acoustic NA of 0.05 [14]. The focused ultrasonic transducer (LiNbO<sub>3</sub> single crystal) had an acoustic NA of 0.2. Both transducers had a center frequency of 40 MHz.

The detected PA signal was amplified and digitized with an analog-to-digital conversion card (ATS-9462 card,

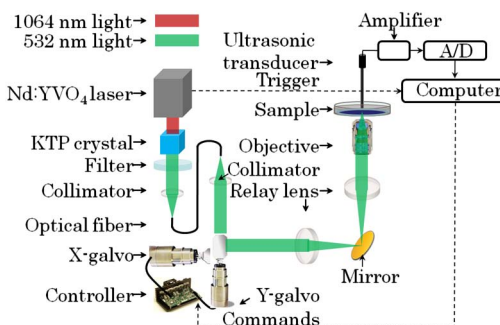


Fig. 1. (Color online) Schematic of the high-speed, high-resolution optical-resolution photoacoustic microscopy system.

Alazar Inc.) housed in a quad-core workstation. For initial alignment, both the sample and the ultrasonic transducer could be manually translated by three-dimensional (3D) mechanical stages that are not shown in Fig. 1. The trigger signal, synchronized with the laser pulses, was sent to the computer as the A-line trigger signal of the imaging system. Commands to the  $x$ - $y$  Galvo scanning system were generated by an NI-6713 card housed in the workstation to control the 2D optical scan. 3D imaging data was streamed to the computer's main random-access memory by a data acquisition thread and was simultaneously delivered to multiple threads for real-time image processing and displaying.

The lateral resolution of the OR-PAM system was determined by the NA of the optical objective [7]. We evaluated the system's lateral resolution by imaging Au nanowire particles (product number 50-30-6000, 30 by 6000 nm, Nanopartz, Inc.). A total of 11 measurements of the line spread function were documented and analyzed for the lateral resolution. The laser beam of 5 nJ energy per pulse was scanned point by point on the sample surface, with 256 A-line measurements at each point. A Gaussian amplitude fitting of the measured line spread function is shown in Fig. 2. The average lateral resolution is  $0.23 \mu\text{m}$ , and the standard deviation is  $0.03 \mu\text{m}$ . The lateral resolution is 2.0 times less than the optical diffraction limit of  $0.45 \mu\text{m}$  ( $0.51\lambda/\text{NA}$ ), probably owing to nonlinear optical absorption of Au nanoparticles and to nonlinear acoustic signal amplification due to laser-generated nanobubbles [15]. This is the first experimental report on super resolution due to apparent phase transition from liquid to vapor.

In order to reduce the jitter of the fast-axis scan mirror during imaging, a sinusoidal waveform was applied on the fast-axis command line. We used only the forward portion of each sinusoidal scan for imaging. An improved imaging protocol using both the forward and backward scan parts will double the imaging speed if the slight misalignment between the forward scan frame and the backward scan frame can be corrected or neglected. The slow axis position was updated before each sinusoidal scan of a B-mode image. The 3D data was usually presented as a 2D maximum amplitude projection (MAP) PA image after interpolation transformation from a sinusoidal scan to a linear scan and assigning the grayscale value as the maximum PA signal amplitude along one A-line perpendicular to the  $X$ - $Y$  plane.

The imaging FOV of the nonfocused ultrasonic transducer was quantified from the 2D MAP PA image [Fig. 3(a)] of a  $500 \mu\text{m} \times 500 \mu\text{m}$  area of the black tape. Two MAP curves are shown in Fig. 3(b) (along the fast axis) and Fig. 3(c) (along the slow axis). Gaussian amplitude fittings of the two plots gave an FWHM FOV of  $326 \mu\text{m}$  along the fast ( $X$ ) axis and  $291 \mu\text{m}$  along the slow ( $Y$ ) axis.

Accordingly, the imaging FOV of the focused ultrasonic transducer was quantified from the 2D MAP PA image [Fig. 3(d)] of a  $150 \mu\text{m} \times 150 \mu\text{m}$  area of the same black tape. Two MAP curves are shown in Fig. 3(e) (along the fast axis) and Fig. 3(f) (along the slow axis). Gaussian amplitude fittings of the two plots gave an FWHM FOV of  $33 \mu\text{m}$  in the fast ( $X$ ) axis direction and  $67 \mu\text{m}$  in the slow ( $Y$ ) axis direction. The asymmetry between the two axes

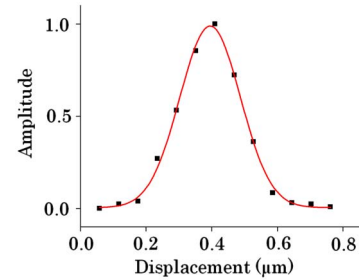


Fig. 2. (Color online) Gaussian amplitude curve fitting of a measured Au nanowire line spread function.

is due to the aspherical focusing of the ultrasonic transducer.

The peak response of the nonfocused ultrasonic transducer was recorded when it was  $650 \mu\text{m}$  away from the black tape sample surface. The peak response of the focused ultrasonic transducer was recorded when it was 2 mm away from the black tape sample surface. The focused ultrasonic transducer provided a 6 dB greater peak response than the nonfocused ultrasonic transducer at the cost of imaging FOV.

To demonstrate cellular imaging, a thin blood smear was prepared, and a  $250 \mu\text{m} \times 125 \mu\text{m}$  patch on the specimen slide was imaged with the stationary, nonfocused ultrasonic transducer with a laser pulse energy of 20 nJ. Each B-scan image had 2048 A-lines. 512 B-mode images

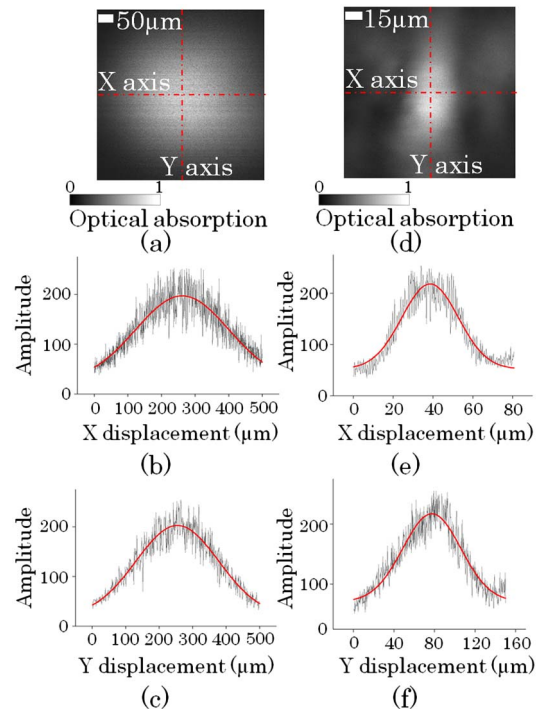


Fig. 3. (Color online) Imaging field-of-view (FOV) calibration: (a) Maximum amplitude projection (MAP) PA image of a black tape patch acquired with the nonfocused ultrasonic transducer. Gaussian amplitude fittings of the MAP PA signals along the (b) fast ( $X$ ) axis and the (c) slow ( $Y$ ) axis give an FWHM FOV of  $326 \mu\text{m}$  along the fast ( $X$ ) axis and  $291 \mu\text{m}$  along the slow ( $Y$ ) axis. (d) MAP PA image of a black tape patch acquired with the focused ultrasonic transducer. Gaussian amplitude fittings of the MAP PA signals along the (e) fast ( $X$ ) axis and the (f) slow ( $Y$ ) axis give an FWHM FOV of  $33 \mu\text{m}$  along the fast ( $X$ ) axis and  $67 \mu\text{m}$  along the slow ( $Y$ ) axis.

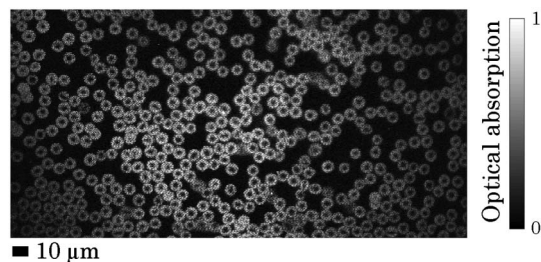


Fig. 4. Maximum amplitude projection (MAP) PA image of RBCs on a  $250\ \mu\text{m} \times 125\ \mu\text{m}$  specimen slide patch.

were acquired for each 3D image. The RBCs in Fig. 4 show opposite contrast to conventional transmission optical microscopy. Shadows at the center of the RBCs are due to their biconcave structures.

The frame rates of the B-mode imaging modes were acquired by measuring the periods of fast-axis scanning waveforms with an oscilloscope. For frame sizes of 4096, 2048, and 1024 A-lines, the frame rates were 22, 43, and 81 Hz, respectively. The ratio of the overhead time to the frame period decreased with increasing frame size.

To demonstrate *in vivo*, real-time, four-dimensional (4D) microcirculation imaging, repeated 2D raster scans of 100 by 50 points on a  $100\ \mu\text{m} \times 50\ \mu\text{m}$  skin patch on a mouse ear were made with a laser pulse energy of 26 nJ. A data set of 256 3D images was continuously recorded in 14.2 s and streamed into a 4D microcirculation movie (Fig. 5, Media 1) provided in the supplemental file. A 4D imaging speed of 18 3D volumes per second was achieved for repeated 2D raster scans of 100 by 50 points. The corresponding 2D B-scan (50 A-lines) frame rate was 1800 Hz while the 1D A-scan rate was 90,000 Hz. A MAP image extracted from the 4D movie is shown in Fig. 5, with flowing RBC clusters identified with red arrows. No damage to the mouse ear tissue was observed after imaging with 40 nJ laser pulse energy [7].

Although imaging speed can be increased as the laser pulse repetition rate is improved, the final imaging speed is limited by practical factors, such as laser safety, imaging depth, and Q-switch noise coupled into the data acquisition system. Our current setup works only in transmission mode, which limits its applications. However, we are developing a reflection-mode system.

In summary, we demonstrated a high-speed, high-resolution OR-PAM system in an inverted microscope configuration with a nanosecond pulsed laser (pulse repetition rate 100,000 Hz) and a stationary ultrasonic transducer. The lateral resolution is  $0.23 \pm 0.03\ \mu\text{m}$  for Au nanowire imaging, which is 2.0 times below the diffraction limit. 4D imaging of microcirculation in a mouse ear was achieved at 18 3D volumes per second for repeated 2D raster scans of 100 by 50 points. The corresponding 2D B-scan (50 A-lines) frame rate was 1800 Hz.

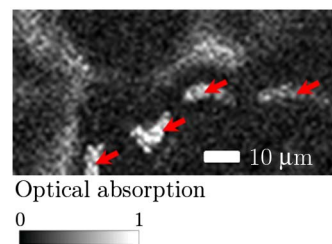


Fig. 5. (Color online) Representative maximum amplitude projection (MAP) PA image of a  $50\ \mu\text{m} \times 25\ \mu\text{m}$  mouse ear patch extracted from a 4D movie (Media 1).

The high imaging speed makes this cellular imaging system suitable for demanding dynamic cellular imaging applications, such as *in vivo* flow cytometry of circulating cancer cells conjugated with Au nanoparticles.

We gratefully thank the National Institutes of Health (NIH) for supporting grants R01 EB000712, R01 EB008085, R01 CA134539, U54 CA136398, R01 CA157277, and P41-EB2182. Help from D. Yao in preparing samples is appreciated. L. Wang has a financial interest in Microphotoacoustics, Inc. and Endra, Inc., which, however, did not support this work.

## References

1. L. V. Wang, *Med. Phys.* **35**, 5758 (2008).
2. L. V. Wang, *Nat. Photon.* **3**, 503 (2009).
3. K. Maslov, H. F. Zhang, S. Hu, and L. V. Wang, *Opt. Lett.* **33**, 929 (2008).
4. G. Ku, K. Maslov, L. Li, and L. V. Wang, *J. Biomed. Opt.* **15**, 021302 (2010).
5. B. Rao, L. Li, K. Maslov, and L. V. Wang, *Opt. Lett.* **35**, 1521 (2010).
6. Z. Xie, S. Jiao, H. F. Zhang, and C. A. Puliafito, *Opt. Lett.* **34**, 1771 (2009).
7. K. Maslov, G. Ku, and L. V. Wang, *Proc. SPIE* **7564**, 75640W (2010).
8. H. F. Zhang, K. Maslov, and L. V. Wang, *Nat. Protoc.* **2**, 797 (2007).
9. S. Hu, B. Rao, K. Maslov, and L. V. Wang, *Opt. Lett.* **35**, 1 (2010).
10. S. Jiao, M. Jiang, J. Hu, A. Fawzi, Q. Zhou, K. K. Shung, C. A. Puliafito, and H. F. Zhang, *Opt. Express* **18**, 3967 (2010).
11. H. F. Zhang, K. Maslov, G. Stoica, and L. V. Wang, *Nat. Biotechnol.* **24**, 848 (2006).
12. J. Yao, K. Maslov, Y. Shi, L. A. Taber, and L. V. Wang, *Opt. Lett.* **35**, 1419 (2010).
13. V. P. Zharov, E. I. Galanzha, E. V. Shashkov, N. G. Khlebtsov, and V. V. Tuchin, *Opt. Lett.* **31**, 3623 (2006).
14. Q. Zhou, X. Xu, E. J. Gottlieb, L. Sun, J. M. Cannata, H. Ameri, M. S. Humayun, P. Han, and K. K. Shung, *IEEE Trans. Ultrason. Ferroelectr. Freq. Control* **54**, 668 (2007).
15. E. I. Galanzha, E. V. Shashkov, P. M. Spring, J. Y. Suen, and V. P. Zharov, *Cancer Res.* **69**, 7926 (2009).